Investigation of the effectiveness of 'multi-harmonic' electron cyclotron current drive in the non inductive EXL-50 ST

Investigation of the effectiveness of ‘multi-harmonic’ electron cyclotron current drive in the non inductive EXL-50 ST

Journal of Physics: Conference Series **2397** (2022) 012011 doi:10.1088/1742-6596/2397/1/012011

Investigation of the effectiveness of 'multi-harmonic' electron cyclotron current drive in the non inductive EXL-50 ST

Debabrata Banerjee

DISAT, Polytechnic University of Turin, Torino 10129, Italy
ENN Science and Technology Development Co. Ltd., Langfang 065001, China

Shaodong Song, Huasheng Xie, Bing Liu, Mingyuan Wang, Wenjun Liu, Bin Chen, Lei Han, Di Luo, Yunyang Song, Xianming Song, Minsheng Liu, Yuejiang Shi, Y. K. Martin Peng and the EXL-50 team

ENN Science and Technology Development Co. Ltd., Langfang 065001, China

Yu. V. Petrov and R. W. Harvey

CompX, Del Mar, CA, USA

E-mail: banerjeed@polito.it

E-mail: shiyuejiang@enn.cn

Abstract.

The fully non-inductive spherical tokamak EXL-50, built and operated by the ENN private limited company, has routinely achieved high current drive efficiency of ~ 1 A/W in only ECRH powered experiments. We have numerically investigated the effectiveness of multiple electron cyclotron resonance (ECR) harmonics in generating such a high efficiency of electron cyclotron current drive (ECCD) in non-inductive plasma start-up. The Fokker-Planck equation is numerically solved to obtain the electron distribution function, under the steady state of relativistic nonlinear Coulomb collision and quasi-linear diffusion operators, for calculating plasma current driven by the injected EC waves. Multi-pass absorption simulations, done with the CQL3D code for extra-ordinary EC waves, demonstrate over 1 A/W efficiency in current for a relatively low density ($\sim 2 \times 10^{18} m^{-3}$), and low temperature ($\sim 100$ eV) plasma, consistent with the experimental results observed on EXL-50. Systematic scanning of different ECR harmonics in simulation has revealed that the multi-harmonic resonance interaction in EXL-50 plays a pivotal role in generating the energetic electron tail responsible for the current.

1. Introduction

The electron cyclotron resonance (ECR) phenomenon governs plasma heating [1, 2] and current drive in tokamak fusion plasma [3, 4], acceleration of electrons [5], and the control of magneto hydrodynamic instability [6]. In some cases, an electron gets opportunity to resonate with multiple harmonics simultaneously to gain much high energy from the wave field, and consequently, its motion becomes stochastic in nature [5]. The generation of energetic electrons by ECR phenomena had also been verified by laboratory experiments in which the 2nd harmonic was found to be more effective than the fundamental ECR [7]. The possibility of non-inductive start-up of a hot plasma current in future large fusion reactors by means of electron cyclotron resonance heating (ECRH) is theoretically investigated recently [8, 9]. An electron, moving with velocity $v_{\parallel}$ along an ambient magnetic field of value B, resonates with the electric field of EC wave propagating with a wave number $k_{\parallel}$, parallel to that magnetic field, via the condition $\omega - k_{\parallel}v_{\parallel} = n\Omega/\gamma$; where γ is the relativistic factor, n stands for the different ECR harmonics and Ω defines the non-relativistic electron cyclotron frequency [10]. Usually, in all conventional tokamaks of large aspect ratio, one or at most two ECR harmonics co-exist inside vacuum vessel. This scenario changes for a new generation low aspect ratio ST which, under purposeful matching of toroidal magnetic field profile and EC wave frequency, contains several ECR harmonics. Such a device named EXL-50, built and owned by the ENN (Energy iNNovation) science and technology development private limited company stationed at Langfang in China, starting its high power operation in the beginning of year 2020 until now, has routinely achieved high current (I_p) drive efficiency (over 1 A/W) in fully non-inductive plasma discharges solely powered by ECRH [11, 12]. There are five number of cold plasma ECR harmonics present inside its vacuum vessel if the toroidal field (TF) coil current is set close to 100 kA. Similarly, high efficiency in plasma current was reported in last two decades on other low aspect ratio devices as well; for example, the LATE [13] and QUEST [14] STs observed high current in ECRH driven fully non-inductive operations (around 75 kA current with about 113 kW injected RF power in QUEST [15]), the MAST device [16] achieved significant amount of current (as high as 73 kA current with upto 60 kW of injected RF power [17]) in electron Bernstein waves driven plasma operation.

In all of these non-inductive ECRH experiments on ST devices, the hard x-ray measurement supports that plasma current is mainly carried by a group of high velocity electrons, known as energetic electrons. However, a complete understanding of the physical mechanism that drives electron to be so energetic and its apparently good confinement in carrying big amount of current remains unachieved. Our effort in the present article is to address this point in light of the effectiveness of multi-harmonic ECRs. A numerical study has been carried out using a Fokker-Plank (FP) code CQL3D [18] in conjunction with a ray-tracing code GENRAY [19] to simulate I_p for a typical EXL-50 discharge. The extra-ordinary EC wave (abbreviated as X-wave or X-mode) is found to be much more efficient than the ordinary EC wave (O-wave or

O-mode) in terms of power deposition and current drive in single-pass simulation. In our study, it is revealed that electrons resonate with multiple harmonics of the X-wave ECR to become highly energetic, and as a result, a significant amount of current is driven. This fact also prevails for muti-pass X-wave simulations as well to generate I_p value in the same order of experimentally measured value. However, the O-mode EC wave simulation has output negligible amount of current even in multi-pass simulation. The role of higher harmonic ECRs for resonating with high energy tail of electron distribution and driving consequently large amount of plasma current becomes more evident in simulation when we step the input power up. This fact is identified to have a probable connection with the quadratic dependence of wave induced quasi-linear (QL) diffusion coefficients on the injected EC wave's electric field. These all results will be presented in detail in the following sections with in-depth analysis and appropriate discussion.

2. EXL-50 plasma powered by electron cyclotron range of frequency (ECRF) wave

The non-solenoidal spherical torus EXL-50 has started operation nearly two years ago. Having envision to explore fully non-inductive long pulse steady state plasma operation, as first step, it utilizes the power of ECRF wave from multiple gyrotrons to startup, heat plasma and subsequently drive current [11]. In a schematic diagram drawn in poloidal cross-section, figure 1(a) shows locations of the six poloidal field coils and three ECRH sources of 28 GHz frequency each - one installed in an equatorial port, and others in an upper mid-plane port being 30 degrees apart from the equatorial one in toroidal direction. A narrow centre post cylinder of radius $\sim$ 17 cm is installed which embraces inner legs of the twelve single turn TF coils capable of conducting upto 100 kA current, but without any solenoidal coils to induce toroidal loop voltage. The hot plasma is kept detached from the device wall with the help of a set of limiters made of tungsten metal installed on the centre post and outboard vessel wall. Also drawn in this diagram are layers of the fundamental and other harmonics (2nd, 3rd, 4th & 5th) of cold plasma ECR present inside the cylindrical shaped vacuum vessel. In the discharge #7672 shown in figure (1b), the closed field lines plasma was found to extend from the fundamental to 4th ECR harmonic, with the 5th one being in open field line plasma region. This discharge is chosen from an experimental campaign on EXL-50 in the last quarter of 2021, when one high power gyrotron (ECRH2) was utilized to inject power (100 - 120) kW, and one low power gyrotron (ECRH1) was used to inject (10 - 20) kW; here the power is measured in the matching optical unit (MOU) that is close to output power from gyrotron. As seen in figure (1b), I_p exhibits a jump after ECRH2 was turned on, then it steadily increases with time to reaching a level more than 1 A/W efficiency. In fact, high plasma current has been routinely observed ranging from 50 kA to 150 kA with the input ECRH power varied from 20 kW upto 120 kW in fully ECRH driven discharges [11]. Line density was measured by a single-chord tangential

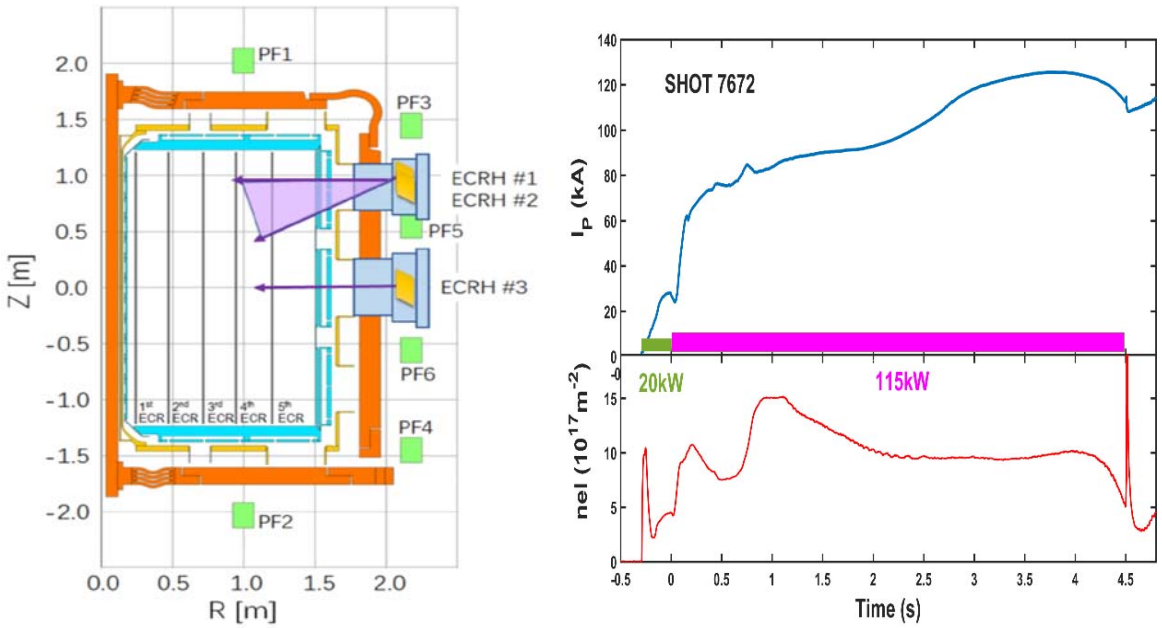

(a) (b)

Figure 1: (a) Schematic diagram of the EXL50 device in poloidal cross-section showing the ports of ECRH sources (in upper and middle planes), locations of six PF coils and the cold ECR harmonic layers as solid black lines. (b) The waveforms of time evolution for one high current drive efficiency discharge #7672. One gyrotron (ECRH1) injected 20 kW from -0.3 s to 0 s and the other gyrotron (ECRH2) injected 115 kW in (0 - 4.5)s duration. I_P and *nel* are the experimentally measured plasma current and line integrated electron density respectively.

microwave interferrometer [20] with its value recorded nearly 1×10^{18} m^{-2} in the flat-top until a sudden peak appeared after the source ECRH2 had been turned off.

ECRH led breakdown and heating of plasma cause to generate a large number of energetic electrons measured by a hard X-ray diagnostic system [11, 21]. In contrary to background highly populated thermal electrons ($<$ 100 eV) mostly being confined within the closed field line plasma, energetic electrons are speculated to roam around in both closed and open field lines plasma regions to carry major portion of plasma current. In full orbit simulations, trajectories of such electrons in the magnetic field structure of these discharges are studied to find that even electrons upto several MeV can be confined inside vacuum vessel. Such dominancy of energetic electrons over thermal electrons was also reported in similar type of experiment performed on LATE [22] and QUEST [14]. Based on experimental finding, one's intuition could be that the thermal and energetic population of electrons perhaps behave as two separate fluids identity of electrons to maintain momentum balance with ions. This ideology has been implemented in a multi-fluid equilibrium code to reconstruct flux information, and thereby estimate plasma current in force balance [12]. Such calculation results in a broadened current density

profile of energetic electrons in plasma covering both closed and open field line regions as shown in figure 8(b) of reference [11]. In a low density, low temperature plasma at which currently EXL-50 is operating, wave power deposition on electrons during first pass is within 10% of the injected power for X-wave, and further one order less for the O-wave, as found in numerical simulation (shown in the next section). Therefore, in the experiment, we may reasonably consider that an EC beam, launched primarily with the O-mode type polarisation from antenna, passes through the plasma many times upon constantly being reflected on the vessel wall made of stainless steel and on limiter surfaces. In reality, the O-mode EC wave has certain probability to convert into other X-mode EC wave upon reflection on a shiny wall with low reflection loss [23]. Therefore, from statistical viewpoint, many times reflected wave may be modeled as having nearly equal probability of being O- and X-wave while it crosses plasma closed flux region many times. Based on this idea, the present article demonstrates multi-pass simulation results considering half of absorbed power attributed to the X-wave, and other half to the O-wave out of the total injected power. The scenario of multi-pass absorptions in the EXL-50 plasma has actually made it quite different from the ECRF wave heated high temperature plasmas in conventional toroidal devices. The generation of large number energetic electrons and their instrumental role towards high current drive efficiency is thought as an outcome of this.

3. Numerical study of the role of multi-harmonic resonances on single-pass absorption

In order to understand the advantage of having multiple number of ECR harmonics co-existed inside EXL-50 plasma over only a single resonance in terms of current drive efficiency, a numerical simulation study has been carried out employing a widely used code CQL3D coupled with another code GENRAY. The CQL3D code [18, 24] has capability to evolve electron distribution function by numerically solving the Fokker-Plank equation in 2D momentum space considering the Coulomb collision and QL diffusion operators as contributing terms. The solution space is set up onto a 2D co-ordinates comprising of momentum along the magnetic field and gyro-averaged momentum across the field. Relativistic Coulomb collisions among thermal and high velocity tail electrons, and electrons with Maxwellian ions are modeled by implementing the Braams-Karney relativistic nonlinear potential functions [25]. Wave-electron interaction is modeled by the well-accepted quasi-linear diffusion theory. To calculate QL diffusion coefficients, all necessary information such as, ray element position, power along rays, electric field polarisation and local magnetic field value, has been generated by ray-tracing simulation in GENRAY [19], and then passed on to CQL3D as input. The bounce averaged FP equation solved in CQL3D for our simulation purpose is expressed as,

$$\lambda \frac{\partial}{\partial t} f_0 \left(u_0, \theta_0, \rho, t\right) = C(f_0) + Q(f_0) \tag{1}$$

where f_0 is the electron distribution as a function of the momentum-per-mass (u_0) and pitch angle (θ_0) at the minimum-B point on each flux surface, ρ the generalized radial coordinate, and t the time. Jacobian $\lambda = v_{\|0}\tau_b$ accounts for the volume of the flux surface occupied per perpendicular area at the midplane, here $v_{\|0}$ stands for parallel speed, and τ_b the bounce (or transit) period. The operator C calculates bounce averaged relativistic nonlinear Coulomb collision effect [25], and Q is the full bounce averaged relativistic Stix QL operator [26]; full mathematical form of these operators can be found in the CQL3D manual [27]. The initial distribution of electrons is considered as Maxwellian which evolves in time to become non-Maxwellian under the play between collision and diffusion operators. All ion species are modeled as background Maxwellian distributions to be engaged in collision with the evolving non-Maxwellian distribution of electrons. The coupled code suite GENRAY-CQL3D was validated successfully by many earlier research studies to predict and explain EC wave heating and current drive experiment on several devices worldwide [28–31].

3.1. Equilibrium setup

The equilibrium is reconstructed based on the PF and TF coil currents, and the plasma current of discharge #7672 to give input magnetic flux profile to GENRAY and CQL3D. As experimentally measured data for density and temperature radial profiles are not available at present, we use model algebraic profiles defined by,

$$n_s = (n_{os} - n_{bs})\,(1 - \rho^{\alpha})^{\beta} + n_{bs}\ ; \quad T_s = (T_{os} - T_{bs})\,(1 - \rho^{\alpha})^{\beta} + T_{bs} \qquad (2)$$

Here, the radial co-ordinate is defined as $\rho = \sqrt{\Phi/\Phi_{lim}}$, Φ being the toroidal flux at respective flux surface, Φ_{lim} the same at last closed flux surface (LCFS). The density and temperature of different species s - meaning electron (e), hydrogen ion (i) and impurities - at the magnetic axis and LCFS are termed as (n_{os}, T_{os}) and (n_{bs}, T_{bs}) respectively. Also importantly, both GENRAY and CQL3D simulations have the same set-up of density, temperature, magnetic field and radial co-ordinate. The EC wave source is characterized in GENRAY by defining launching parameters similar to the experimental set-up i.e., the upper-plane source ECRH2 launches 115 kW power at frequency 28 GHz directed at 15 degrees poloidal angle relative to horizontal plane at the antenna location, and also obliquely in toroidal plane by an angle of 5 degrees with normal injection. The power across different rays is divided based on a Gaussian profile dependence on ray angle around the central ray of the beam. Another important parameter to be defined in simulation is the injected beam width, which is kept sufficiently wide (size of plasma minor radius) to match the relatively less focused beam at antenna.

3.2. O-wave of 28GHz frequency

With this setup of EC ray-launch, and $n_s - T_s$ profiles as shown in figure (2c), the GENRAY code was run first to perform ray-tracing to generate informations for calculating QL diffusion coefficients. Next, the CQL3D code was run with the same

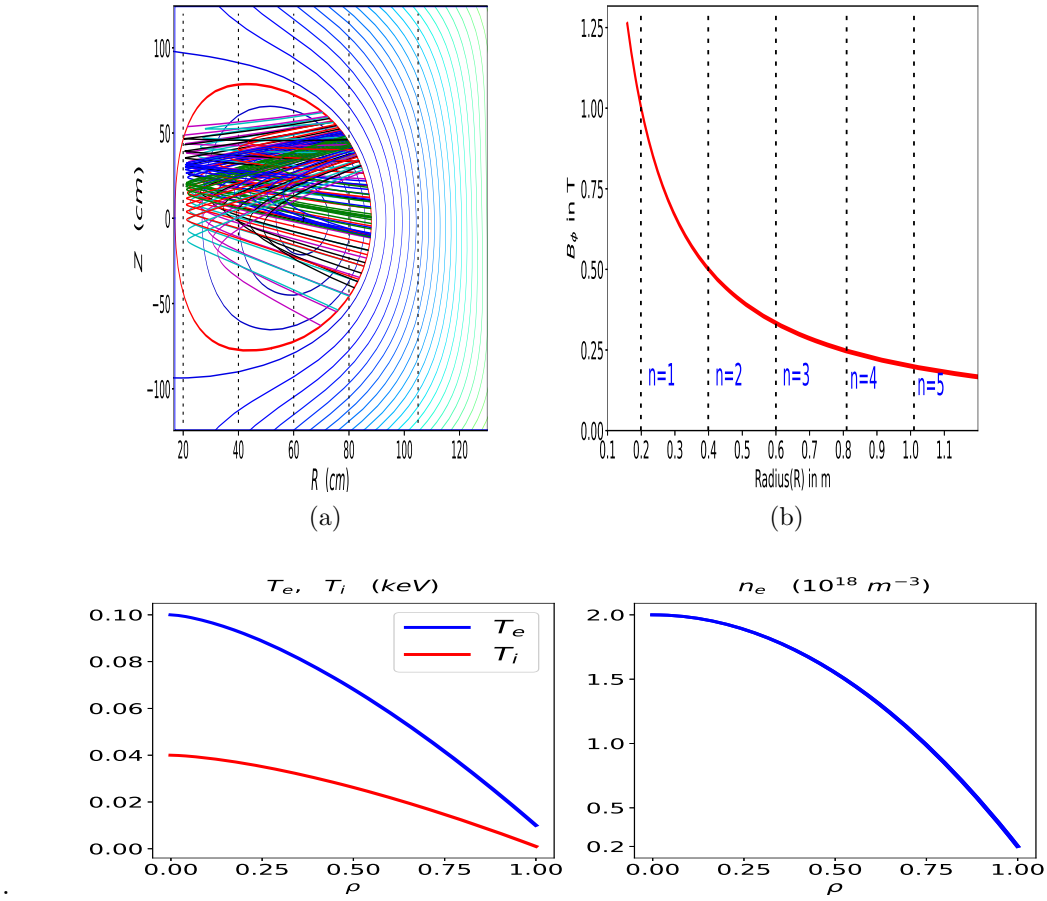

Figure 2: (a) Contour plot of poloidal flux with illustration of the X-mode ray-trajectory and cold plasma ECR harmonic layers. (b) toroidal magnetic field vs. major radius with the cold ECR harmonic locations. (c) Assumed profiles of species density and temperature following equation (2), core electron density $n_{oe} = 2 \times 10^{18}\ m^{-3}$, core electron temperature $T_{oe} = 100$ eV, core ion temperature $T_{oi} = 40$ eV. For $Z_{eff} = 1$, $n_{oe} = n_{oi}$. For $Z_{eff} > 1$, density of hydrogen ion and other impurity ions are adjusted so that all ions' cumulative density equals electron density maintaining quasi-neutrality, and temperatures of impurity ions are kept same with that of H-ion.

density and temperature profiles, and the same equilibrium field setup to solve equation (1), and to calculate absorbed power and plasma current. As the polarisation of injected EC beam in experiment was primarily of O-wave type, we first have studied single pass absorption for O-mode root of the cold plasma dispersion relation in ray-tracing simulation. In CQL3D run, QL diffusion coefficients are calculated for total 5 harmonics ($n = 1 - 5$) - from the fundamental ($n = 1$) upto the 5th ECR harmonic ($n = 5$) - in similarity with the number of cold ECR harmonics present inside EXL-50 as shown

in figure 2 (a,b). Absorbed power density profile with minor radius (ρ) in figure 3(a) indicates absorption around the cold 2nd harmonic ECR at $\rho = 0.5$ being stronger than that around the fundamental ECR ($n = 1$) at $\rho = 0.9$, even though damping for the fundamental ECR be stronger than on 2nd harmonic based on the ECRH theory prediction. This is because the $n = 1$ cold resonance layer lies near to $\rho = 1$ (LCFS) accessing much lower plasma temperature compared to the $n = 2$ layer. On other hand, we know from ECRH theory that power deposition on $O2$ is at least one order lower than $X2$ for same density and temperature.

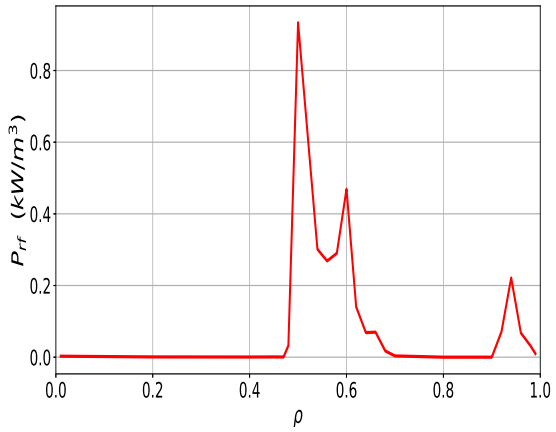

(a) harmonic n=2 is at $\rho = 0.5$, n=1 at $\rho = 0.95$

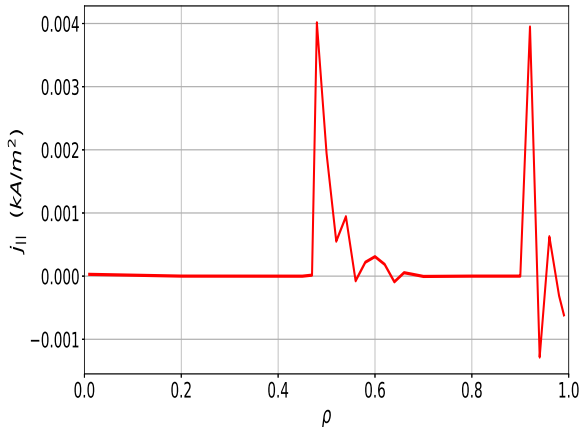

(b) harmonic n=2 is at $\rho = 0.5$, n=1 at $\rho = 0.95$

Figure 3: O-wave power deposition profile (a), and current density profile (b) from CQL3D solution. Both profiles are localized around the fundamental and 2nd harmonic cold ECRs.

Therefore, a significantly lower amount of absorbed power (20 W on $O1$, 280 W on $O2$ and negligible amount at higher harmonics $n = 3 - 5$) has come out from CQL3D run. As a result, driven plasma current at all harmonics is negligibly small (figure 3(b)), projecting O-wave to be inefficient in driving an initial low density and low temperature plasma in our ST. This run amounts to a trivial current 0.2 A with basically no feature of multi-harmonic influence. This fact will be further confirmed by multi-pass simulation results in the next section. The electron distribution function (f_e), as it has emerged from the steady state solution of equation (1), remains almost unchanged from the initial Maxwellian form (2D plot in figure 4(a), and 1D cuts of f_e at constant pitch angles in figure 4(b)) without forming any energetic electron tail. Besides, we checked running simulations for different toroidal and poloidal launch angles but haven't found any improvement in current drive efficiency of the O-wave. This fact of the poor efficiency of O-wave in depositing power resembles with a recent ray-tracing simulation study on QUEST [15]. Such finding has let us to investigate the efficacy of X-wave which may appear in present experiment via the mode conversion from O- to X-wave upon reflection on wall.

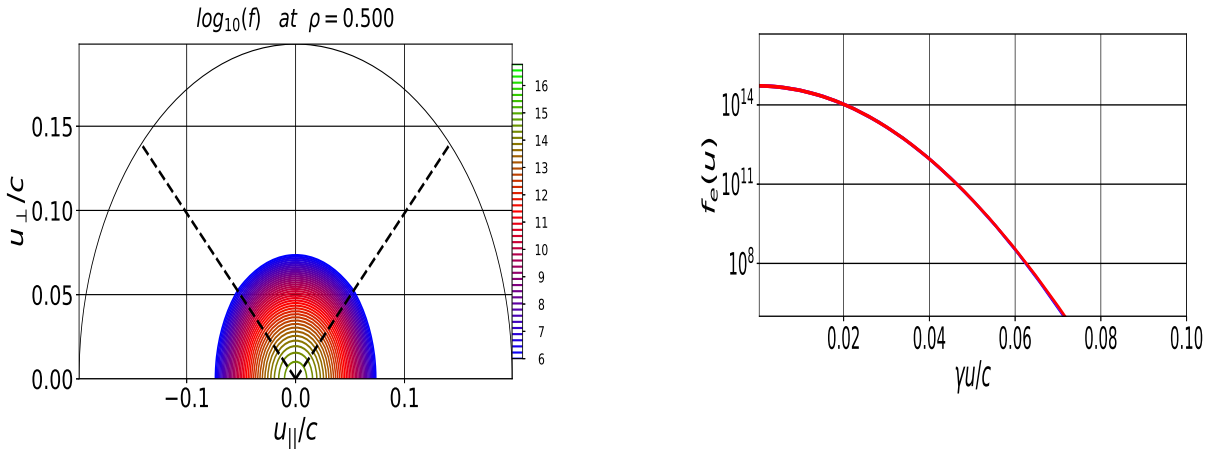

(a) (b)

Figure 4: (a) electron distribution function in relativistic $\mathbf{u}/c \equiv \mathbf{p}/mc$ space computed with CQL3D for the O-wave. Final solution remains almost equal to the starting Maxwellian form. (b) cuts through the 2D electron distribution function f_e (of figure 4(a)) at four different constant pitch angles vs. $\gamma u/c$, γ being the relativistic factor.

3.3. X-wave of 28GHz frequency

Unlike the O-wave, similar type of numerical study with the X-wave has found high effectiveness of multi-harmonic EC resonances in current drive. Considering the same base parameters of magnetic field, density and temperature described in figure 2, and equal wave launching set-up such as input power, frequency, injection angles and beam width used for the O-wave study, we have conducted ray-tracing in GENRAY for the X-mode branch of cold plasma dispersion, and then solved the FP equation in CQL3D. EXL-50 being operated with limiters and having inboard limiters neck to neck with the cold plasma fundamental resonance layer, has high presence of impurities such as helium (He), carbon (C) etc. Keeping in mind that the resulting increased effective ion charge Z_{eff} can alter electron distribution and thus affect plasma current, we have decided to run simulations for two values of $Z_{eff} = 2.5$ & 4.0. Although, a real value is not available from diagnostic measurements, this assumed value $Z_{eff} = 4.0$ is expected to be close to the experimental one of discharge #7672. As shown in figure (2a), all rays marked in different colours are reflected on the right hand cut-off frequency layer before reaching the fundamental resonance location as per the X-wave's cold plasma dispersion characteristic. To investigate the effectiveness of all harmonics in detail, we increase the number of harmonics step by step in CQL3D input following this order: 1st simulation run using only the fundamental harmonic, 2nd run with $n = 1-2$ harmonics i.e. the fundamental and 2nd harmonics together, and so on upto the 5th run with

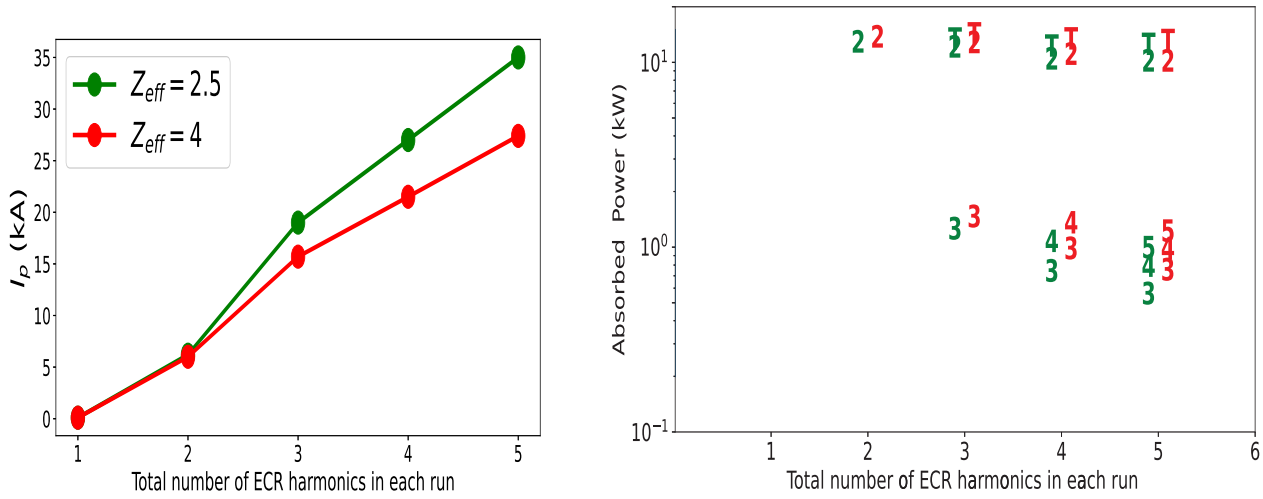

(a) (b)

Figure 5: (a) The rise in plasma current with increasing number of ECR harmonics. The meaning of abscissa is described in subsection (3.3), (b) power sharing among harmonics for each run; mode numbers from each run are shown on graph at the corresponding absorbed power vertical location, green colour for $Z_{eff} = 2.5$ and red for $Z_{eff} = 4.0$. The total absorbed power from each run is marked on the figure as 'T'.

$n = 1 - 5$ harmonics. Toroidal plasma current obtained from CQL3D in every run is plotted against the respective simulation run number in figure 5(a) for both values of Z_{eff}. Current in the first run at which only the fundamental harmonic is involved comes out zero due to no resonance occuring between the wave vector and electron velocity around the $n = 1$ harmonic layer. Being the dominant one in terms of power deposition, 2nd harmonic in the 2nd run amounts to 6.2 kA current for $Z_{eff} = 2.5$ and 6 kA for $Z_{eff} = 4.0$. As we add on higher harmonics, I_p for $Z_{eff} = 2.5$ (green line) and $Z_{eff} = 4.0$ (red line) quickly ramps up with contribution from harmonics $n = 3 - 5$. Power and current density profiles are seen as localized around the 2nd harmonic cold ECR location within $\rho = 0.48 - 0.6$, even for the cases those include harmonics higher than $n = 2$ in calculation (figure 6). It may be interpreted that, as per the ECRH theory, electrons moving around the cold 2nd ECR location resonate with it to absorb high amount of wave power. Associated with this, a high value of the asymmetric QL diffusion generates long tail of electron velocity distribution via the pitch angle scattering of long range Coulomb interaction. Thus created energetic electrons eventually resonate with higher harmonics ($n > 2$) by means of a two-step mechanism; first, through the relativistic Doppler shifted resonance and second, via a nonlinear interaction with different harmonics. The first step is widely interpreted as being effective for power absorption in fully EC wave powered operation on QUEST [15]. This article explores the nonlinear second step that comes owing to the quadratic dependence of QL diffusion coefficients on wave electric field. The sharing of total absorbed power among different

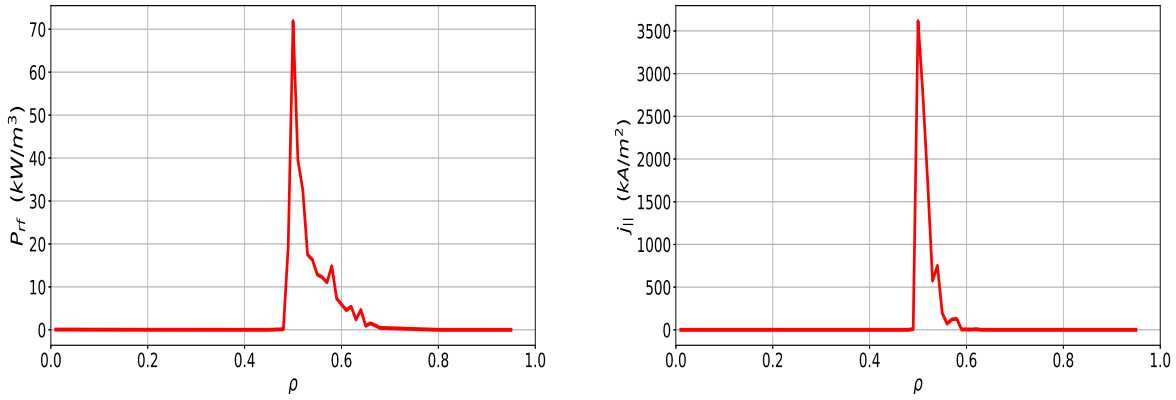

(a) harmonic n=2 is at $\rho = 0.5$ (b) harmonic n=2 is at $\rho = 0.5$

Figure 6: Power deposition (a) and current density (b) with minor radius in case of X-wave from the run $n = 1 - 5$, $Z_{\text{eff}} = 4.0$. Both profiles are localized around the cold 2nd harmonic ECR layer.

harmonics in every run is displayed in figure 5(b). A large fraction of power goes to the 2nd harmonic in each run with a gradual drop in its value as more number of harmonics are getting involved.

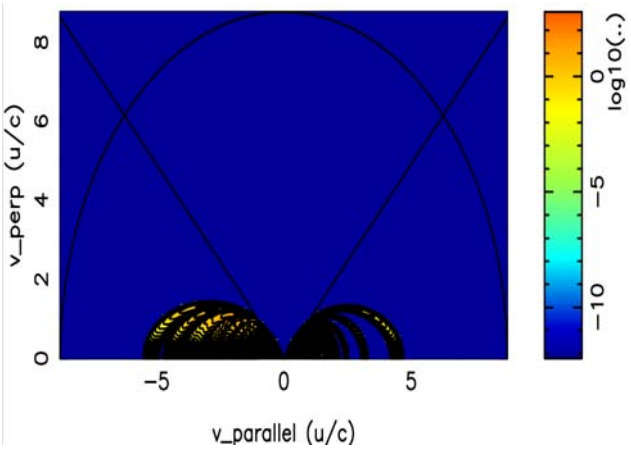

(a) (b)

Figure 7: (a) Quasi-linear diffusion coefficient in relativistic $\mathbf{u}/c \equiv \mathbf{p}/mc$ space computed with CQL3D in case of X-wave for the 3rd harmonic (a) and for the 5th harmonic (b) from a run $n = 1 - 5$, $Z_{\text{eff}} = 4.0$. The diffusion is generally high away from the t-p boundary (solid black straight lines), but $n = 5$ harmonic exhibits diffusion across the t-p boundary into trapped particle region.

In CQL3D, Z_{eff} appears in the Coulomb collision calculation between electrons and different impurity ion species. The QL diffusion coefficient in 2D velocity space is

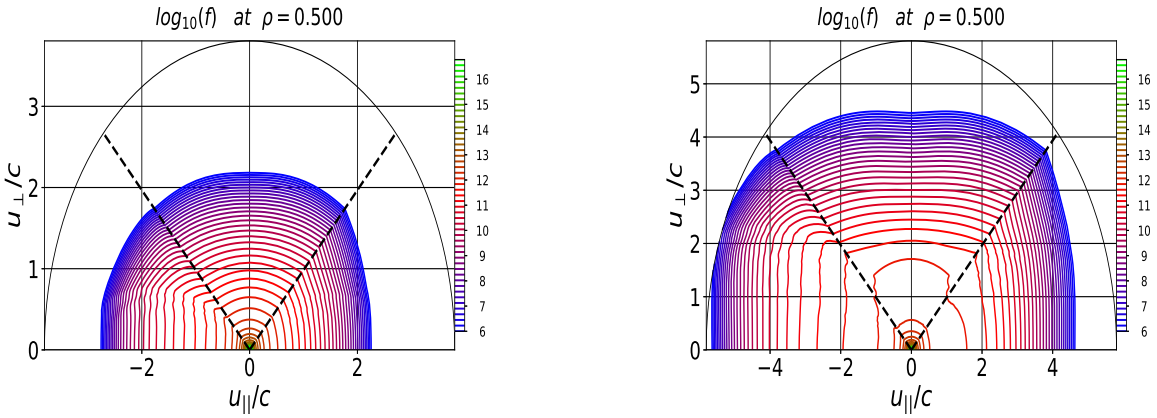

(a) f_e from n=1-2 run (b) f_e from n=1-5 run

Figure 8: Electron distribution function (f_e) in relativistic $\mathbf{u}/c \equiv \mathbf{p}/mc$ space computed with CQL3D for the X-wave; (a) f_e, $n = 1-2$, $Z_{eff} = 4.0$; (b) f_e, $n = 1-5$, $Z_{eff} = 4.0$. Both distribution functions are fetched from minor radius location $\rho = 0.5$.

plotted in figure 7 for the harmonics third and fifth from a simulation run for $n = 1-5$ harmonics. Figure 7(a) clearly shows diffusion is more evident in passing particle region away from the trapped-passing (t-p) boundary, and it is asymmetric being dominant for velocity opposite to local magnetic field. Diffusion property changes noticeably for the 5th harmonic as it enters trapped region by crossing t-p boundary, and further extends to high velocity regime (figure 7(b)). Important characteristic to note is the maximum diffusion location (intense coloured region in plots) moves further to higher velocity region with the increasing order of ECR harmonic. In figure 8, distribution functions in velocity space are shown for the two runs $n = 1-2$ and $n = 1-5$. There is clear asymmetry in high velocity region and the most distinguishable asymmetric line in distribution for the $n = 1-5$ case is lying more close to the t-p boundary compared to the $n = 1-2$ case. From a case study of $Z_{eff} = 4.0$ and $n = 1-5$, we have demonstrated the different nature of distribution functions at three radial locations - at $\rho = 0.01$ near to the 3rd harmonic cold ECR (figure 9(a)), at $\rho = 0.5$ near to the 2nd harmonic cold ECR (figure 9(b)), at $\rho = 0.9$ near to the 4th harmonic position (figure 9(c)). Clearly, $\rho = 0.5$ location contains a long tail of high velocity electron population in addition to a low temperature bulk thermal population. But, no such tail is visible in electron distribution at $\rho = 0.01$ or $\rho = 0.9$. It is due to weak resonance between thermal electrons and the 3rd & 4th harmonic ECRs at low temperature (< 100 eV).

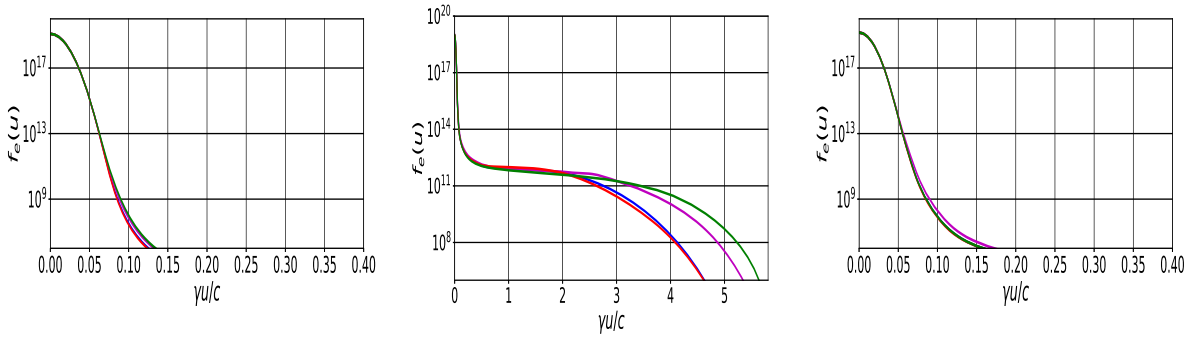

(a) X3 resonance at $\rho = 0.01$ (b) X2 resonance at $\rho = 0.5$ (c) X4 resonance at $\rho = 0.9$

Figure 9: cuts at four different constant pitch angles through the 2D electron distribution function f_e taken from three different radial locations (a) $\rho = 0.01$, (b) $\rho = 0.5$, (c) $\rho = 0.9$ vs. $\gamma u/c$, where γ is the relativistic factor. $\rho = 0.5$ position characterizes a long tail of distribution compared to other two locations.

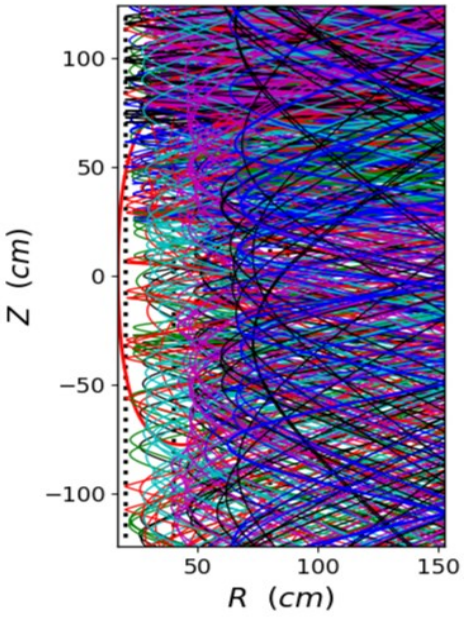

Figure 10: Ray-tracing diagram in poloidal plane from the multi-pass X-mode simulation with 36 times reflection on wall. Rays have covered entire 2D space including both open and closed field line regions.

4. Modeling of Multi-pass absorptions with the 28 GHz EC wave reflecting on wall

As explained in section (2), a multi-pass absorption simulation is inevitable to fully represent a low density, low temperature experimental scenario of EXL-50. The GENRAY code's capability of tracing multi-pass ray propagation with ray-reflection occurred on simulation boundary (representing vessel wall) is implemented in this section. Now, rays are visible to be in both inside and outside the LCFS basically filling up nearly the full volume of simulation domain as drawn in figure 10. However,

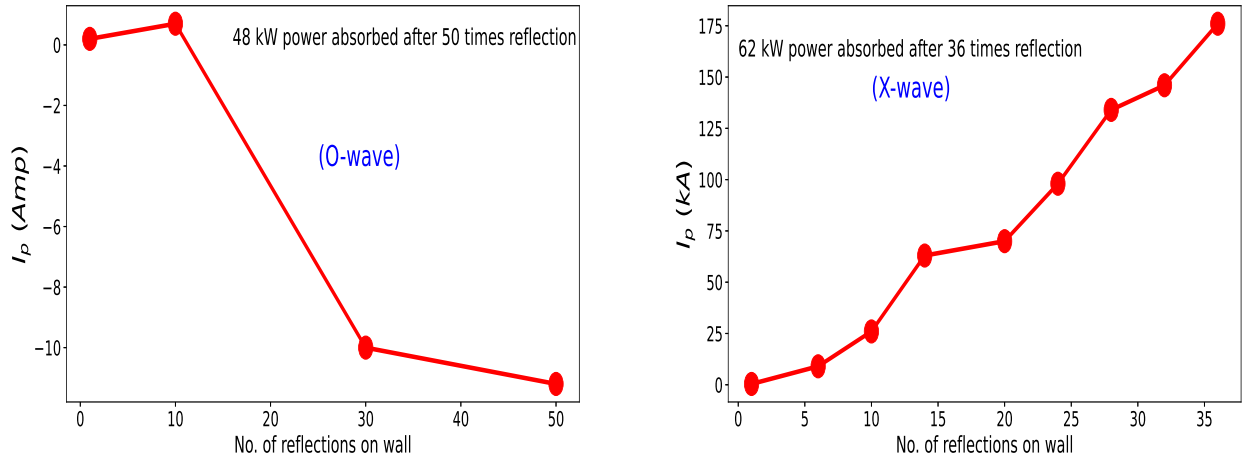

(a) (b)

Figure 11: (a) I_p vs. number of reflection on wall for O-wave multi-pass runs. The generated current in this case is of negligible amount eventhough in total $\sim$ 48 kW power has been absorbed. (b) I_p vs. number of reflection on wall for X-mode multi-pass runs. I_p rises with step wise increase of reflection numbers finally reaching to $\sim$ 175 kA level in expense of $\sim$ 62 kW input power.

CQL3D being a bounce averaged code in poloidal direction can only deal with a closed field line plasma. Therefore, current flowing along open field lines in EXL-50 can't be simulated with it at present. Nevertheless, this section may help us understand current drive mechanism inside the closed field plasma region for multi-pass absorptions. Like single-pass ray-tracing in section (3), magnetic field profiles are fetched from discharge #7672, density and temperature profiles are set like as figure 2 with only change in the core density value $n_{eo} = 1 \times 10^{18}\ m^{-3}$, aiming for the low line integrated density value of discharge #7672.

Multi-pass simulations are conducted separately for both O- & X-waves with injecting 115 kW input power from the ECRH2 launcher for each case. Since the wave polarisation may change from being O- to X- mode type or vice versa upon reflection on the device wall, and such mode conversion is not currently modeled in GENRAY, two

sets of multi-pass simulation are carried out separately for the O- & X-wave by gradually increasing number of reflections until nearly half of the input power is found absorbed for each wave. Figure 11(b) provides us the information that about 175 kA current is driven in expense of 62 kW input power absorbed, after as many as 36 times reflection on simulation boundary have occurred for the X-mode EC wave. On other hand, a merely

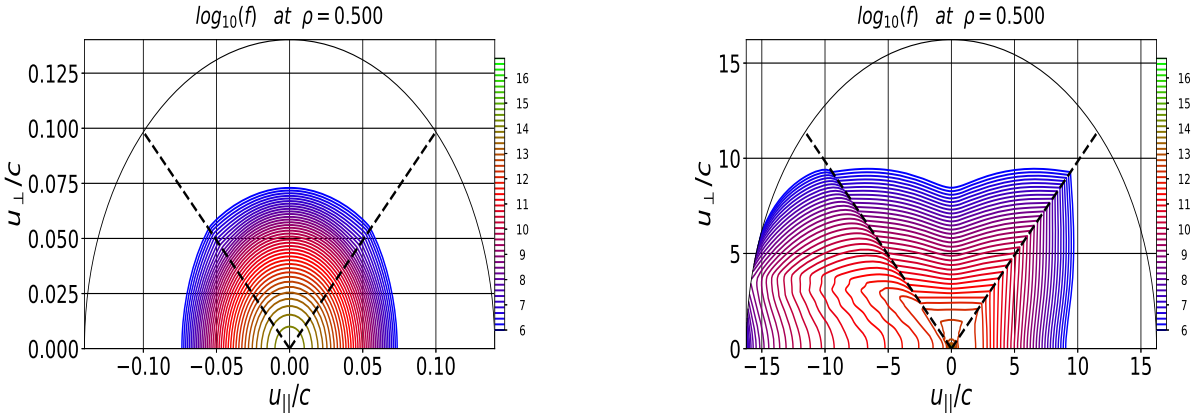

(a) debu (b)

Figure 12: Electron distribution function (f_e) in relativistic $\mathbf{u}/c \equiv \mathbf{p}/mc$ space computed with CQL3D for multi-pass absorption. (a) f_e from the O-mode run performing 50 times reflection, (b) f_e from the X-mode run performing 36 times reflection on the simulation boundary.

10 Amp counter current is flown in the case of O-wave while 48 kW power is absorbed after 50 times reflection. Here, total absorbed power includes power due to collisional damping and reflection loss on wall in GENRAY alongwith the power deposition via wave-electron resonance. Even though this cumulative current is a little exaggeration of the experimental steady state current 125 kA achieved in shot #7672, the order of estimation might be acceptable given the fact that real power sharing between the O-wave and X-wave is hard to speculate in multi-pass scenario in experiment, and the precise values of density, temperature and Z_{eff} at resonance locations are not available at present. From the contour plots of electron distribution function at the final stage of simulation for both O- & X-waves in figure 12(a,b), we may understand the reason that makes these two cases so different from each other, as the X-wave diffusion is highly asymmetric whereas the O-wave diffusion is almost symmetric in co- and counter-direction of $u_{\|}/c$.

5. Discussions

In the X-wave single-pass simulation, inclusion of multiple harmonics in calculation is found to strengthen current drive efficiency of the EC wave. This has happened

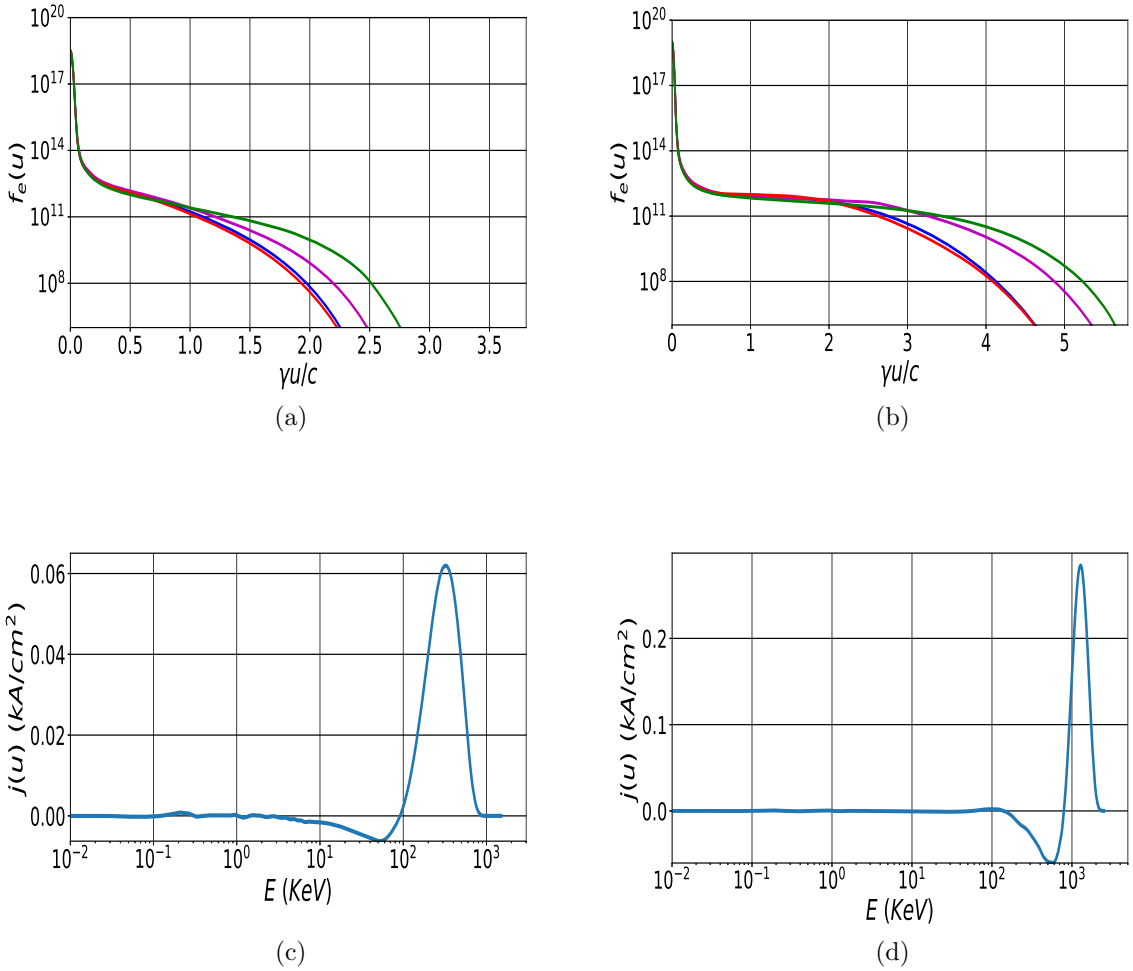

Figure 13: Cuts at four different constant pitch angles through the 2D electron distribution function f_e taken from two different case studies - (a) $n = 1 - 2,\ Z_{\text{eff}} = 4.0$ (b) $n = 1 - 5,\ Z_{\text{eff}} = 4.0$ vs. $\gamma u/c$, where γ is the relativistic factor. For same runs current density function $j(u)$ vs. energy of electrons for $n = 1 - 2$(c) & $n = 1 - 5$(d). Total current density at respective radial position is $\int j(u)du$ with u being in normalized unit.

because high velocity electrons around the cold 2nd ECR location ($\rho = 0.5$) resonate strongly with higher harmonics ($n > 2$) as per the relativistic Doppler shifted resonance condition to become more and more energetic and, as a result, drive higher current. We can visualize this fact in figure 13(a,b) where the $n = 1 - 5$ run extends electron distribution tail further out in the high velocity limit compared to the $n = 1 - 2$ run. Also, current density function in velocity plotted in figure 13(c,d) manifests the same that current in the $n = 1 - 5$ run is carried by comparatively higher energy electrons than the $n = 1 - 2$ run. This characteristic prevails in multi-pass simulation for the X-wave as presented in detail in the preceding section. On other hand, this feature is

absent from the O-wave multi-pass simulation result, eventhough all plasma and wave input parameters are kept exactly same with the X-wave simulation set-up. It is likely because the power deposition of O-wave on the 2nd harmonic is much weaker than that of the X-wave, what can't produce high velocity electron tail to resonate with higher harmonics.

It is well known, from the earlier studies of particle acceleration via wave-particle interaction, charged particle may accelerate to very high velocity by means of "overlapping of resonances" mechanism if the wave electric field exceeds stochasticity threshold [5], and consequently, the motion of charged particle may lead to diffusion in velocity space [32]. Farina and co-authors [33] also reported that a local QL form of diffusion coefficient could accurately model this diffusive character of electron's motion. We think such physical mechanism may support our result of generation of energetic electron via multi-harmonic resonance that is obtained by numerically solving the FP equation with QL diffusion coefficients. However, this conjecture needs to be verified through further theoretical and numerical analysis, beyond the scope of present article though.

Recent simulation studies on the QUEST ST [15, 35] - an EC wave driven non-inductive plasma operation similar to EXL-50 - has also investigated the dominancy of energetic electron fraction over the bulk thermal electron population in absorbing EC-wave power, and predicted the usefulness of multi-harmonic on current drive by examining the relativistic ECR condition in high energy domain. In another modeling of non-inductive plasma current [36], it was reported, in their terminology, minority hot electrons by the 2nd harmonic ECR power absorption could drive most of the current observed on QUEST. Our recent study of ray-tracing simulation on EXL-50 also confirmed that the single pass absorption ratio of X- to O-wave can be larger than 50% with around 2% energetic electrons of few hundreds keV energy [37]. In all of these studies, various energetic electron parameters - its distribution, temperature and density - are presumed and set through a mathematical function with some informations collected from experiments. However, in our present study, energetic electron tail has been formed by solving the FP equation in time starting with an initial low temperature ($< 100eV$) Maxwellian distribution. This numerical study has revealed an effective mechanism of "multi-harmonic interaction" that may explain high current drive efficiency for EXL-50. Now, making assessment of how close our present simulation effort has been to match with the actual experiment on EXL-50, we may emphasize our result being consistent with the finding in experiment. However, there are some features, those may be influential in reality but could not be implemented in this work such as,

- No model is included to simulate current flowing along the open field line region. But, in reality, plasma may have a part of current outside the closed flux region as identified on basis of a multi-fluid modeling [12].
- Radial diffusion of electrons is not considered in our modeling, that could expand the highly localized current density profile formed in simulation.

- Orbital loss mechanism for fast electrons that has been found important in describing current on MAST [38] and LATE [23] is also not modeled here.

6. Summary

In our simulation study, by applying the Fokker-Plank, quasi-linear theory, the same high efficiency in current (over 1 A/W) has been obtained in presence of multi-harmonic ECRs similar to the experimental observation on EXL-50. This is because energetic electrons resonate with multiple higher harmonics via the relativistic Doppler shift. The effectiveness of higher harmonics ($n > 2$) is found significant when the input wave power exceeds a threshold value, suggesting it to depend on the quadratic nonlinearity of wave electric field in the QL diffusion coefficient. Also found is that plasma current increases significantly in multi-pass absorptions compared to single-pass absorption in simulation, indicating the beneficial role of multi-reflection of EC waves inside the vacuum vessel [39]. In experiment [11], a set of discharges was performed varying the toroidal launch angle of antenna but the usual dependence of current on injection angle as known from the RF wave current drive theory was not detected. The reason behind such angle insensitivity of toroidal current is not understood so far on basis of this simulation result. A question prevails to verify the validity of the quasi-linear theory for such low temperature plasma filled with high power RF waves. A previous study on the same issue for DIII-D tokamak found that the quasilinear theory would work accurate until injected RF power was not very high [40]. The current density profile emerged from this modeling is highly localized radially which differs from our observation of a broader profile in experiment, encompassing both the closed and open field regions [12]. The absence of radial diffusion calculation of electrons across flux surfaces in our present model could possibly be a reason behind this outcome. It may also arise due to inability of CQL3D to track energetic electrons which eventually travel from closed to open field lines, and remain confined. In this regard, a complete model considering EC wave driven current in open field lines remains a necessity to develop in future. Further research will be carried out in experiment and modeling to better understand this mechanism of 'multi-harmonic interaction' and improve the performance of EXL-50 operation.

Acknowledgment

We sincerely thank Dr. Houyang Guo (ENN) for his assistance of careful reading the manuscript and commenting on it. DB highly appreciates Dr. Bihe Deng's (ENN) interesting questions on the physics content, and acknowledges encouragement by Mr. Baoshan Yuan (ENN). This work was performed under the auspices and full support of the compact fusion project granted by the ENN group, China. Yu .V. Petrov was supported by the US Department of Energy under grant DE-FG02-04ER54744.

References

[1] Prater R 2004 *Phys. Plasmas* **11** 2349
[2] Karney C F F 1978 *Phys. Fluids* **21** 1584
[3] Luce T C *et al.* 1999 *Phys. Rev. Lett.* **83** 4550
[4] Harvey R W *et al.* 1997 *Nucl. Fusion* **37** 69
[5] Menyuk C R 1988 *Phys. Fluids* **31** 3768
[6] Harvey R W and Perkins F W 2001 *Nucl. Fusion* **41** 1847
[7] Ikegami H *et al.* 1973 *Nucl. Fusion* **13** 351
[8] Maekawa T *et al.* 2018 *Nucl. Fusion* **58** 016037
[9] Maekawa T *et al.* 2018 *Nucl. Fusion* **58** 106020
[10] Erckmann V and Gasparino U 1994 *Plasma Phys. Control. Fusion* **36** 1869–1962
[11] Shi Y *et al.* 2022 *Nucl. Fusion* **62** 086047
[12] Ishida A *et al.* 2021 *Phys. Plasmas* **28** 032503
[13] Maekawa T *et al.* 2005 *Nucl. Fusion* **45** 1439–1445
[14] Idei H *et al.* 2017 *Nucl. Fusion* **57** 126045
[15] Onchi T *et al.* 2021 *Phys. Plasmas* **28** 022505
[16] Shevchenko V F *et al.* 2010 *Nucl. Fusion* **50** 022004
[17] Shevchenko V F *et al.* 2015 *EPJ Web of Conf.* **87** 02007
[18] Harvey R W and McCoy M G 1992 The cql3d fokker-plank code proc. of iaea tcm montreal, June 15-18
[19] Harvey R W 1994 *Bull. Am. Phys. Soc.* **39** 1626
[20] Li S J *et al.* 2021 *JINST* **16**
[21] Cheng S K *et al.* 2021 *Rev. Sci. Instrum.* **92** 043513
[22] Uchida M *et al.* 2010 *Phys. Rev. Lett.* **104** 065001
[23] Maekawa T *et al.* 2012 *Nucl. Fusion* **52** 083008
[24] Kerbel G D and McCoy M G 1985 *Phys. Fluids* **28** 3629
[25] Braams B J and Karney C F F 1989 *Phys. Fluids* 1355
[26] Stix T H 1992 *Waves in Plasmas* (New york: AIP)
[27] Harvey R W and McCoy M G 1992 The cql3d fokker-plank code (https://www.compxco.com/cql3d_manual.pdf)
[28] Prater R *et al.* 2008 *Nucl. Fusion* **48** 035006
[29] Harvey R W *et al.* 2002 *Phys. Rev. Lett.* **88** 205001
[30] Zheng P *et al.* 2018 *Nucl. Fusion* **58** 036010
[31] Petty C C *et al.* 2002 *Nucl. Fusion* **42** 1366
[32] Smith G R and Kaufman A N 1978 *Phys. Fluids* **21** 2230
[33] Farina D *et al.* 1994 *Phys. Plasmas* **1** 1871
[34] Shi Y *et al.* 2021 Solenoid-free current drive via ecrh in exl-50 spherical torus plasmas arXiv:2104.14844
[35] Kojima S *et al.* 2021 *Plasma Phys. Control. Fusion* **63** 105002
[36] Ono M *et al.* 2020 *AIP Conf. Proc.* **2254** 090001
[37] Xie H S *et al.* 2004 *Comput. Phys. Commun.* **276** 108363
[38] du Toit E J *et al.* 2017 *EPJ Web of Conf.* **147** 01002
[39] Banerjee D *et al.* 2021 Investigation of the effectiveness of non-inductive 'multi-harmonic' electron cyclotron current drive through modeling multi-pass absorptions in the exl-50 spherical tokamak under review in Nuclear Fusion
[40] Harvey R W and Prater R 2001 *AIP Conf. Proc.* **595** 298